THE JOURNAL OF PHYSICAL CHEMISTRY Letters

Letter

pubs.acs.org/JPCL

Metrological Investigation of the (6,5) Carbon Nanotube Absorption Cross Section

Laura Oudjedi,[†,‡] A. Nicholas G. Parra-Vasquez,[†,‡,§] Antoine G. Godin,[†,‡] Laurent Cognet,[†,‡] and Brahim Lounis*[,†,‡]

[†]University of Bordeaux, LP2N, F-33405 Talence, France

[‡]CNRS & Institut d'Optique, LP2N, F-33405 Talence, France

Supporting Information

ABSTRACT: Using single-nanotube absorption microscopy, we measured the absorption cross section of (6,5) carbon nanotubes at their second-order optical transition. We obtained a value of 3.2×10^{-17} cm^2/C atom with a precision of 15% and an accuracy below 20%. This constitutes the first metrological investigation of the absorption cross section of chirality-identified nanotubes. Correlative absorption–luminescence microscopies performed on long nanotubes reveal a direct manifestation of exciton diffusion in the nanotube.

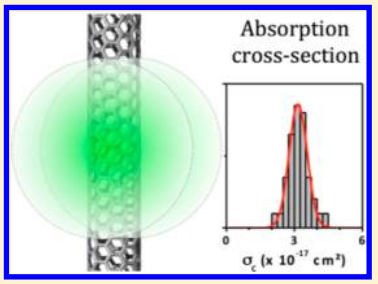

SECTION: Physical Processes in Nanomaterials and Nanostructures

Single-wall carbon nanotubes (SWCNTs) provide unique opportunities for applications in electronics, optoelectronics, photonics, and photovoltaics.[1] They are indeed nearly ideal models of infinite π-orbital conjugations where the sp^2 lattice provides exceptional charge carrier properties.[2] Moreover, their true one-dimensional character confers them well-defined optical transitions from excitonic states[3,4,5] While their Raman and photoluminescence properties have been extensively studied,[5] the basic absorption properties of SWCNTs are still poorly established in a quantitative manner, even if they are of prime importance for applications. Indeed, common absorption measurements on ensembles of SWCNTs suffer from the problem of samples heterogeneities inherent to standard synthesis methods. The large multiplicity of nanotube chiralities and lengths, as well as the presence of synthesis impurities, impede the ability to assess the exact amount of a SWCNT's chirality contributing to an absorption signature. For (6,5) nanotubes, absorption cross sections σ_C ranging from 0.5×10^{-18} to 1.3×10^{-17} cm^2/C atom can be deduced from previous reports[6−9] considering an excitation light polarized along the nanotubes and resonant with the second-order transition (S_{22}). The majority of the caveats mentioned above that are responsible for the disparity in σ_C determination can be lifted off by performing measurements on individual SWCNTs.

Single SWCNT absorption measurements are challenging because the weak signals have to be extracted from laser intensity fluctuations (including the always present shot noise) and contributions from environment scattering.[10] Luminescence microscopy, which is an intrinsic dark field method, has been used to perform the first evaluation of σ_C for individual (6,5) nanotubes. The method was based on the study of the luminescence dependence with excitation intensity, which deviates from linearity at high excitation due to exciton–exciton annihilation processes.[11] From the saturation intensity and the luminescence lifetime of the SWCNT, σ_C was estimated to be $\sim 10^{-17}$ cm^2/C atom.[11] However, individual defects that are photoinduced upon increasing excitation intensity quench the luminescence and therefore can strongly alter the saturation behavior.[12,13] The Rayleigh intensity scattering technique combined with AFM has been used to extract an estimate of $\sim 2.5 \times 10^{-17}$ cm^2/C for the resonant absorption cross section of nanotubes of different diameters.[14] Recently, a value in the range of $\sim 10^{-17}$ cm^2/C was reported for a large diameter (18,5) nanotube lying on an opaque substrate excited around its S_{33} transition using a reflective modulation imaging technique.[15]

Given the large disparity in the reported absorption cross section values, a metrological approach is essential to provide a definitive value. Here, we present a quantitative measurement of the absorption cross section of chirality-identified individual (6,5) nanotubes at their S_{22} transition peak. We choose the (6,5) chirality as standard nanotubes because they can easily be identified by their luminescence spectra and be excited efficiently near their second-order resonance S_{22} using low-noise CW solid-state lasers. Futhermore, they are widely studied because of their abundance in standard synthesis methods (CoMoCAT or HiPco for instance) and because their luminescence falls in the detection window of silicon detectors. Our direct measurement of the carbon nanotube absorption cross section requires assumption on neither the sample content nor data interpretation. It was made possible by

Received: February 15, 2013
Accepted: April 4, 2013
Published: April 4, 2013

   dx.doi.org/10.1021/jz4003372 | J. Phys. Chem. Lett. 2013, 4, 1460−1464

combining transmission microscopy for absorption determination with luminescence microscopy for chirality assignment and photothermal microscopy for assuring nanotube isolation.

We optimize the transmission spatial modulation technique[16] to detect the extinction cross section of small-diameter SWNTs with high signal-to-noise ratios. For small-diameter SWCNTs, the extinction cross section is dominated by the absorption, as demonstrated by Rayleigh scattering experiments, which reported scattering cross sections 2 orders of magnitude smaller than absorption cross sections for (6,4) nanotubes.[14] One limiting factor of this technique was that only relatively low frequencies (<kHz) could be used for modulating the sample position due to mass loading.[17] Thus, these measurements suffer from $1/f$ noise. Our approach is based on a high-frequency (f = 100 kHz) spatial modulation of a tightly focused Gaussian beam across the nanoobject (Figure 1). In practice,

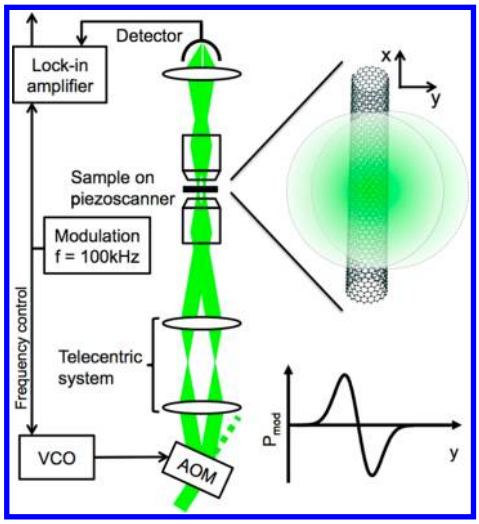

Figure 1. Schematics of the experimental setup. A sample placed at the focal plane of a microscope objective and containing isolated nano-objects (gold nanoparticles or carbon nanotubes) is mounted on a piezoscanner. An acousto-optic modulator (AOM) is used to modulate the position of the exciting beam in the sample plane (beam modulation amplitude of 36 nm along the y axis at 100kHz). The transmitted beam is collected by a second microscope objective and sent to a fast photodiode connected to a lock-in amplifier. The signal is the demodulated power P_{mod} as a function of the sample position. A typical profile shape of P_{mod} along the y axis is illustrated (see the text).

the spatial modulation of a 561 nm laser beam is performed by varying the first-order diffraction angle of an acousto-optic modulator. The incident beam is focused onto the sample by means of a high NA microscope objective (60×, NA 1.45), and its transmission collected by a second identical objective is sent to a balanced photodetector connected to a lock-in amplifier for demodulation. Images of the samples are obtained by raster scanning the sample mounted on a piezoscanning stage.

The sensitivity and metrological potential of the method is first validated on a standard nanosphere sample. This sample consists of gold nanoparticles (NPs) with a mean diameter of 10.0 ± 0.8 nm (measured on 191 NPs by TEM; Figure 2a,b) deposited on a cleaned glass coverslip, embedded in immersion oil for index matching (~1.50). In the case of small nano-objects, the extinction cross section is dominated by the absorption[18] (negligible intensity scattering). For a small spherical gold NP (with dimensions much smaller than the wavelength) at the position (x,y), the transmitted beam power

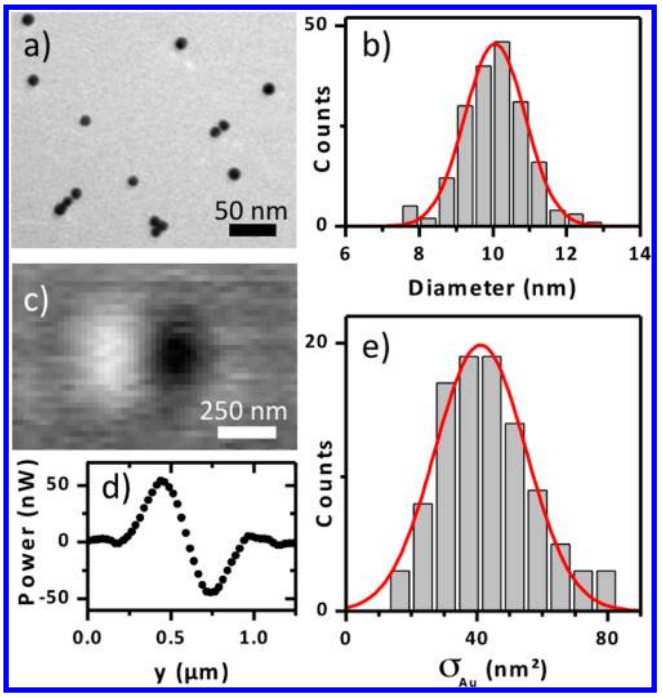

Figure 2. (a) TEM image of a 10 nm individual gold NP used in this study. (b) Histogram of the diameters measured on 191 NPs and its Gaussian fit.(c) Modulated absorption image of a single 10 nm gold NP excited at 561 nm (P_0 = 650 μW, 25 ms/pixel). (d) Corresponding profile averaged over four lines of (c). (e) Histogram of the absorption cross sections deduced for 100 individual 10 nm gold NPs with its Gaussian fit (see the text).

is $P_{trans}(t) = P_{inc} - \sigma_{Au} I(x,y + \delta \sin(2\pi f t))$, with P_{inc} as the incident beam power, σ_{Au} as the NP absorption cross section, $I(x,y)$ as the intensity profile at the sample, and δ as the amplitude of the spatial modulation along the y axis. Assuming a Gaussian beam profile

$$I(x', y') = I_0 e^{\frac{-2(x'^2+y'^2)}{w_0^2}}$$

and a small beam modulation amplitude ($\delta \ll w_0$), the demodulated power is proportional to the beam profile first derivative along the y axis and is written as

$$P_{mod}\left(x, y\right) = -\frac{8y}{\pi w w_0^4}\sigma_{Au}\delta \times P_{inc} e^{\frac{-2(x^2+y^2)}{w_0^2}}$$

As shown in Figure 2c,d, individual gold nanoparticles are imaged with a high signal-to-noise-ratio (>20) with short integration times of 25 ms and an excitation power of 650 μW.

It follows that σ_{Au} can be directly measured from the peak-to-peak amplitude A_{pp} of the profile ($\sigma_{Au} = (\pi e^{1/2}/8)(w_0^3/\delta)(A_{pp}/P_{inc})$), given the precise determination of the beam size w_0 and displacement δ.

For this purpose, the beam profile was determined by confocal fluorescence images of 45 individual 20 nm luminescent spheres deposited on a glass coverslip (Figure 1S, Supporting Information). We find w_0 = 269 ± 6 nm (mean ± standard deviation). The beam displacement at the sample is calibrated by measuring the displacement of individual quantum dot positions found in two confocal images acquired with two different RF waves driving the acousto-optic modulator (Figure 2S, Supporting Information). From 13

dx.doi.org/10.1021/jz4003372 | J. Phys. Chem. Lett. 2013, 4, 1460−1464

acquisitions, we found δ = 36.4 ± 1.9 nm (mean ± standard deviation).

After careful calibration of the demodulated signal, one obtains a mean absorption cross section for 10 nm gold NPs of 41 ± 16 nm^2 (mean ± half-width at half-maximum, N = 191) at a 561 nm excitation wavelength (Figure 2e). This is in excellent agreement with the value of 42 nm^2 predicted by Mie theory[18,19] for a particle surrounded by a medium with a refraction index of 1.50. Noteworthy, the dispersion in the measured NP absorption cross section (33%) is mainly imposed by the NP size dispersion (30% in volume) because the measurement uncertainties play a minor role here (see below). This measurement demonstrates that our experimental procedure allows quantitative determination of small nano-object absorption cross sections.

We then consider (6,5) SWCNTs to achieve precise characterization of their absorption cross section. Raw HiPco SWCNTs were solubilized in 1% aqueous sodium deoxycholate (DOC) using brief tip sonication followed by benchtop centrifugation to remove unsolubilized material from the suspension. Nanotubes were deposited on a cleaned glass coverslip and covered with immersion oil for further analysis. In order to identify long individual (6,5) SWCNTs, single-molecule wide-field photoluminescence (PL) microscopy was first performed with a detection window around their S_{11} emission transition (985 nm).[20] Figure 3a shows a bright individual (6,5) nanotubes displaying uniform luminescence.

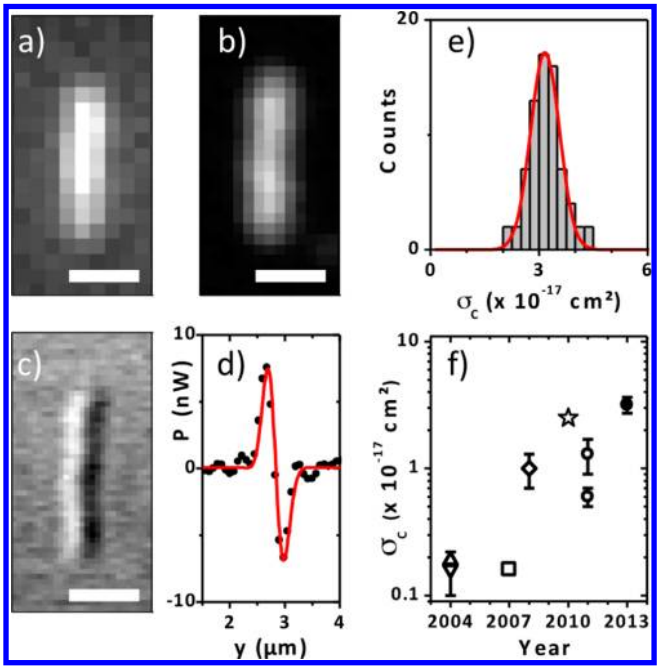

Figure 3. Luminescence (a, 300 ms integration time), photothermal (b, 5 ms/pixel), and modulated absorption (c, 25 ms/pixel) images of the same individual (6,5) carbon nanotube. Scale bars are 1 μm. (d) Absorption profile perpendicular to the nanotube axis averaged over 10 lines of (c). (e) Histogram of the absorption cross sections deduced for 71 individual (6,5) carbon nanotubes and its Gaussian fit (see text). The mean value of the distribution is 3.2 × 10^{-17} cm^2, and its standard deviation is 0.5 × 10^{-17} cm^2. (f) Comparison with the values reported in the literature for (6,5) nanotubes (all values were normalized to an excitation at the S_{22} transition with a polarization along the nanotube axis): Δ, ref 6; ∇, ref 7; □, ref 8; ◇, ref 11; ○, ref 9; ☆, ref 14; ●, this work.

The selected nanotubes were then imaged using the modulated absorption method. Because the signal amplitude and profile depend on the nanotube orientation with respect to the beam modulation axis, the measurements were performed only on long nanotubes perpendicular to the y axis (Figure 3b). Furthermore, the laser polarization was set along the nanotube for maximum interaction.[21] To ensure that the nanotubes were isolated from other nanotube species or from catalyst impurities, always abundant in nanotubes samples, we performed photothermal heterodyne microscopy on the same sample region.[22,23] In this case, we used circularly polarized excitation to obtain images independent from tube orientations (Figures 2c and 3S, Supporting Information). The perfect correlation between PL, photothermal, and modulated absorption images allows assignment of the individual (6,5) nanotubes without ambiguities.

In contrast to gold nanoparticles, which can be considered infinitely small compared to the beam profile, the 1D geometry of the nanotube has to be taken into account in the derivation of demodulated power

$$P_{\mathrm{mod}}(x,y) = -\sqrt{\frac{8}{\pi}}\frac{\delta}{w_0^3}P_{\mathrm{inc}}n_C\sigma_C y e^{-2y^2/w_0^2}\left[\mathrm{erf}\left[\frac{\sqrt{2}}{w_0}\left(x+\frac{L}{2}\right)\right]-\mathrm{erf}\left[\frac{\sqrt{2}}{w_0}\left(x-\frac{L}{2}\right)\right]\right]$$

where L is the SWCNT length and n_C the number of carbon atoms per tube length (n_C = 88271 μm^{-1} for (6,5) nanotubes). Figure 3d displays the signal profile $P_{\mathrm{mod}}(x = 0,y)$ along the y axis measured around the middle part of the tube at an excitation power of 70 μW.

In the case of nanotubes significantly longer than the diffraction limit (i.e., L > 1 μm), σ_C can be expressed as a function of A_{pp} using $\sigma_C = [(2\pi)^{1/2}e^{1/2}/8](w_0^2/n_C\delta)(A_{\mathrm{pp}}/P_{\mathrm{inc}})$. The excitation laser wavelength is not strictly resonant with the S_{22} transition; one has to account for the dependence of the absorption on the excitation wavelength to provide a value for σ_C at the peak of this transition. For this purpose, we acquired photoluminescence excitation (PLE) of individual (6,5) nanotubes prepared following the same sample procedure as that for absorption measurements because the optical spectra depend on the nanotube local environment. A tunable dye laser (emission range 540−590 nm) was used for excitation, and the SWCNT luminescence signal was recorded at low excitation intensities to avoid any saturation effect. PLE spectra displayed systematically a Lorentzian profile[24] with a peak S_{22} transition found at 569 ± 2 nm (Figure 4S, Supporting Information). From eight spectra acquired, a correction factor of 1.47 ± 0.12 is deduced, allowing the determination of σ_C at the S_{22} peak transition using the measurements performed with a low-noise solid-state laser at 561 nm. Figure 3e displays the histogram σ_C measured on 73 different (6,5) nanotubes. A unimodal distribution is obtained, providing a clear signature that all data points stem from individual chirality-identified nanotubes. The histogram is well adjusted with a Gaussian distribution centered at 3.2 × 10^{-17} cm^2 with a half-width at half-maximum of 0.5 × 10^{-17} cm^2. This value compares to the upper range of previous indirect estimations of σ_C (Figure 3f).[14] Importantly, this obtained value originates from direct measurements (model-independent); therefore, we can determine both its precision and its exactitude in a straightforward manner. The relative error in the predetermination of w_0 (2%, which

dx.doi.org/10.1021/jz4003372 | J. Phys. Chem. Lett. 2013, 4, 1460−1464

translates to 4% error on σ_C), δ (5%), and the excitation wavelength correction factor (9%) might induce a systematic bias on the determination of σ_C, thus affecting its exactitude by up to 18%. Furthermore, we estimate the precision of this measured value to be 15%, stemming from a 10% noise-to-signal ratio for A_{pp}, a 1% precision in the determination of the beam power, and 2% fluctuations on w_0 due to sample-to-sample focusing. We thus conclude that the measured spread of the data (±16%) displayed in Figure 4b reflects the precision of the determination of σ_C, while its exactitude lies within 18%.

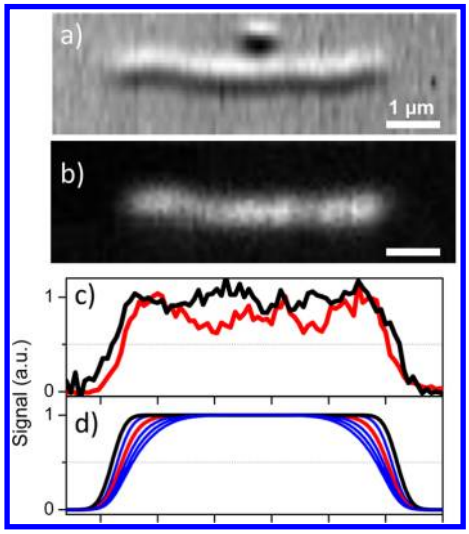

Figure 4. Confocal microscopy images ((a) modulated absorption; (b) luminescence, 50 ms/pixel) of an individual (6,5) carbon nanotube using the same excitation beam. (c) Corresponding absorption (black) and luminescence (red) profiles along the nanotube axis. (d) Simulated profiles using a 1D diffusion equation (see the text and Supporting Information): absorption (black) and photoluminescence (red and blue) for varying diffusion lengths (100 to 500 nm). The best agreement with experiments is obtained for l_D = 200 nm (red).

Correlative imaging (luminescence versus absorption) of a long carbon nanotube provides direct evidence of exciton diffusion and a straightforward determination of the exciton diffusion length l_D before its recombination.[25,26] Previous determinations rely on stepwise quenching of nanotube luminescence by chemical reactions,[27,28] by ensemble studies of the length dependence of PL efficiency,[29] or on studying the luminescence spatial profile at nanotube ends.[30] In the latter case, determination of l_D relies on fitting carefully the intensity profile at the nanotube end where local quenching occurs.

Here, we show that by simultaneous acquisition of the luminescence and absorption profiles, l_D can be directly determined by confronting the apparent nanotube ends between the two imaging modalities. To this aim, individual nanotubes were imaged by confocal luminescence and spatial modulation absorption microscopies with the same confocal excitation beam (Figure 4a,b). Comparison of the images reveals that nanotube PL profiles appear systematically shorter than absorption ones (Figure 4c). This is a direct consequence of exciton diffusion. The apparent nanotube ends appear separated by ~150 nm between the two images. Using a simple 1D exciton diffusion model (Supporting Information) with quenching at the nanotube ends, we simulated the expected PL and absorption profiles obtained in our confocal microscope for l_D varying from 0 to 500 nm. The best agreement with the experiments is found for $l_D \approx 200$ nm (Figure 4d). This value is in agreement with previous determinations for a nanotube suspended in DOC.[30,31]

In conclusion, we measured the absorption cross section of (6,5) carbon nanotubes at their second-order optical transition and obtained a value of 3.2×10^{-17} cm^2 per carbon atom. This constitutes the first metrological investigation of the absorption cross section of chirality-identified nanotubes. Besides its importance for fundamental investigations of nanotube physical properties (e.g., accurate determination of exciton rate generation), this value is also essential for carbon nanotube material science and a key parameter for exploiting the large application potential that nanotubes offer in optoelectronics and photovoltaics.

■ ASSOCIATED CONTENT

Ⓢ Supporting Information

Laser beam profile and displacement determination, selection of isolated (6,5) nanotubes, photoluminescence excitation spectra at the S_{22} transition of individual (6,5) nanotubes, and steady-state exciton concentration calculation with laser scanning microscopy modality. This material is available free of charge via the Internet at http://pubs.acs.org.

■ AUTHOR INFORMATION

Author Contributions

§A.N.G.P.-V.: Los Alamos National Laboratory, Los Alamos, NM 87545.

Notes

The authors declare no competing financial interest.

■ ACKNOWLEDGMENTS

We thank Morgane Gandil for experimental help. This work was funded by the Agence Nationale de la Recherche, Région Aquitaine, DGA, and the European Research Council.

■ REFERENCES

(1) De Volder, M. F. L.; Tawfick, S. H.; Baughman, R. H.; Hart, A. J. Carbon Nanotubes: Present and Future Commercial Applications. *Science* **2013**, *339*, 535−539.

(2) Avouris, P.; Appenzeller, J.; Martel, R.; Wind, S. J. Carbon Nanotube Electronics. *Proc. IEEE* **2003**, *91*, 1772−1784.

(3) Wang, F.; Dukovic, G.; Brus, L. E.; Heinz, T. F. The Optical Resonances in Carbon Nanotubes Arise from Excitons. *Science* **2005**, *308*, 838−41.

(4) Maultzsch, J.; Pomraenke, R.; Reich, S.; Chang, E.; Prezzi, D.; Ruini, A.; Molinari, E.; Strano, M. S.; Thomsen, C.; Lienau, C. Exciton Binding Energies in Carbon Nanotubes from Two-Photon Photoluminescence. *Phys. Rev. B* **2005**, *72*, 241402R.

(5) Jorio, A.; Dresselhaus, G.; Dresselhaus, M. S. *Carbon Nanotubes: Advanced Topics in the Synthesis, Structure, Properties & Applications*; Springer: Berlin, New York, 2008; p 720.

(6) Islam, M. F.; Milkie, D. E.; Kane, C. L.; Yodh, A. G.; Kikkawa, J. M. Direct Measurement of the Polarized Optical Absorption Cross Section of Single-Wall Carbon Nanotubes. *Phys. Rev. Lett.* **2004**, *93*, 037404.

(7) Zheng, M.; Diner, B. A. Solution Redox Chemistry of Carbon Nanotubes. *J. Am. Chem. Soc.* **2004**, *126*, 15490−15494.

(8) Carlson, L. J.; Maccagnano, S. E.; Zheng, M.; Silcox, J.; Krauss, T. D. Fluorescence Efficiency of Individual Carbon Nanotubes. *Nano Lett.* **2007**, *7*, 3698−3703.

(9) Schöppler, F.; Mann, C.; Hain, T. C.; Neubauer, F. M.; Privitera, G.; Bonaccorso, F.; Chu, D.; Ferrari, A. C.; Hertel, T. Molar Extinction Coefficient of Single-Wall Carbon Nanotubes. *J. Phys. Chem. C* **2011**, *115*, 14682−14686.

(10) Lefebvre, J.; Finnie, P. Polarized Light Microscopy and Spectroscopy of Individual Single-Walled Carbon Nanotubes. *Nano Res.* **2011**, *4*, 788−794.
(11) Berciaud, S.; Cognet, L.; Lounis, B. Luminescence Decay and the Absorption Cross Section of Individual Single-Walled Carbon Nanotubes. *Phys. Rev. Lett.* **2008**, *101*, 077402.
(12) Georgi, C.; Hartmann, N.; Gokus, T.; Green, A. A.; Hersam, M. C.; Hartschuh, A. Photoinduced Luminescence Blinking and Bleaching in Individual Single-Walled Carbon Nanotubes. *ChemPhysChem* **2008**, *9*, 1460−1464.
(13) Santos, S. M.; Yuma, B.; Berciaud, S.; Shaver, J.; Gallart, M.; Gilliot, P.; Cognet, L.; Lounis, B. All-Optical Trion Generation in Single-Walled Carbon Nanotubes. *Phys. Rev. Lett.* **2011**, *107*, 187401.
(14) Joh, D. Y.; Kinder, J.; Herman, L. H.; Ju, S.-Y.; Segal, M. A.; Johnson, J. N.; ChanGarnet, K. L.; Park, J. Single-Walled Carbon Nanotubes as Excitonic Optical Wires. *Nat. Nanotechnol.* **2011**, *6*, 51−56.
(15) Christofilos, D.; Blancon, J. C.; Arvanitidis, J.; Miguel, A. S.; Ayari, A.; Del Fatti, N.; Vallée, F. Optical Imaging and Absolute Absorption Cross Section Measurement of Individual Nano-objects on Opaque Substrates: Single-Wall Carbon Nanotubes on Silicon. *J. Phys. Chem. Lett.* **2012**, *3*, 1176−1181.
(16) Arbouet, A.; Christofilos, D.; Del Fatti, N.; Vallee, F.; Huntzinger, J. R.; Arnaud, L.; Billaud, P.; Broyer, M. Direct Measurement of the Single-Metal-Cluster Optical Absorption. *Phys. Rev. Lett.* **2004**, *93*, 127401.
(17) Carey, C. R.; LeBel, T.; Crisostomo, D.; Giblin, J.; Kuno, M.; Hartland, G. V. Imaging and Absolute Extinction Cross-Section Measurements of Nanorods and Nanowires through Polarization Modulation Microscopy. *J. Phys. Chem. C* **2010**, *114*, 16029−16036.
(18) Bohren, C. F.; Huffman, D. R. *Absorption and Scattering of Light by Small Particles*. John Wiley: New York, 1983.
(19) Mie, G. Beiträge zur Optik Trüber Medien, Speziell Kolloidaler Metallösungen. *Ann. Phys.* **1908**, *330*, 377−445.
(20) Duque, J. G.; Pasquali, M.; Cognet, L.; Lounis, B. Environmental and Synthesis-Dependent Luminescence Properties of Individual Single-Walled Carbon Nanotubes. *ACS Nano* **2009**, *3*, 2153−2156.
(21) Lefebvre, J.; Finnie, P. Polarized Photoluminescence Excitation Spectroscopy of Single-Walled Carbon Nanotubes. *Phys. Rev. Lett.* **2007**, *98*, 167406.
(22) Berciaud, S.; Cognet, L.; Blab, G. A.; Lounis, B. Photothermal Heterodyne Imaging of Individual Nonfluorescent Nanoclusters and Nanocrystals. *Phys. Rev. Lett.* **2004**, *93*, 257402.
(23) Berciaud, S.; Cognet, L.; Poulin, P.; Weisman, R. B.; Lounis, B. Absorption Spectroscopy of Individual Single-Walled Carbon Nanotubes. *Nano Lett.* **2007**, *7*, 1203−1207.
(24) Cambré, S.; Santos, S. M.; Wenseleers, W.; Nugraha, A. R. T.; Saito, R.; Cognet, L.; Lounis, B. Luminescence Properties of Individual Empty and Water-Filled Single-Walled Carbon Nanotubes. *ACS Nano* **2012**, *6*, 2649−2655.
(25) Wang, F.; Dukovic, G.; Knoesel, E.; Brus, L. E.; Heinz, T. F. Observation of Rapid Auger Recombination in Optically Excited Semiconducting Carbon Nanotubes. *Phys. Rev. B* **2004**, *70*, 241403(R).
(26) Ma, Y. Z.; Valkunas, L.; Dexheimer, S. L.; Bachilo, S. M.; Fleming, G. R. Femtosecond Spectroscopy of Optical Excitations in Single-Walled Carbon Nanotubes: Evidence for Exciton−Exciton Annihilation. *Phys. Rev. Lett.* **2005**, *94*, 1.
(27) Cognet, L.; Tsyboulski, D. A.; Rocha, J. D.; Doyle, C. D.; Tour, J. M.; Weisman, R. B. Stepwise Quenching of Exciton Fluorescence in Carbon Nanotubes by Single-Molecule Reactions. *Science* **2007**, *316*, 1465−1468.
(28) Cognet, L.; Tsyboulski, D. A.; Weisman, R. B. Subdiffraction Far-Field Imaging of Luminescent Single-Walled Carbon Nanotubes. *Nano Lett.* **2008**, *8*, 749−753.
(29) Hertel, T.; Himmelein, S.; Ackermann, T.; Stich, D.; Crochet, J. Diffusion Limited Photoluminescence Quantum Yields in 1-D Semiconductors: Single-Wall Carbon Nanotubes. *ACS Nano* **2010**, *4*, 7161−7168.
(30) Crochet, J. J.; Duque, J. G.; Werner, J. H.; Lounis, B.; Cognet, L.; Doorn, S. K. Disorder Limited Exciton Transport in Colloidal Single-Wall Carbon Nanotubes. *Nano Lett.* **2012**, *12*, 5091−5096.
(31) Siitonen, A. J.; Tsyboulski, D. A.; Bachilo, S. M.; Weisman, R. B. Surfactant-Dependent Exciton Mobility in Single-Walled Carbon Nanotubes Studied by Single-Molecule Reactions. *Nano Lett.* **2010**, *10*, 1595−1599.